CHEMISTRY OF MATERIALS

Open Access

pubs.acs.org/cm

Article

Probing the Local Structure of Na in $NaNO_3$-Promoted, MgO-Based CO_2 Sorbents via X-ray Absorption Spectroscopy

Margarita Rekhtina, Aram Bugaev, Matthew T. Dunstan, Alessandro Dal Pozzo, Manouchehr Nadjafi, Camelia Borca, Thomas Huthwelker,* Paula M. Abdala,* and Christoph R. Müller*

Cite This: *Chem. Mater.* 2023, 35, 10060−10069

Read Online

ACCESS | Metrics & More | Article Recommendations | Supporting Information

ABSTRACT: This work provides insight into the local structure of Na in MgO-based CO_2 sorbents that are promoted with $NaNO_3$. To this end, we use X-ray absorption spectroscopy (XAS) at the Na K-edge to interrogate the local structure of Na during the CO_2 capture ($MgO + CO_2 \leftrightarrow MgCO_3$). The analysis of Na K-edge XAS data shows that the local environment of Na is altered upon MgO carbonation when compared to that of $NaNO_3$ in the as-prepared sorbent. We attribute the changes observed in the carbonated sorbent to an alteration in the local structure of Na at the $NaNO_3/MgCO_3$ interfaces and/or in the vicinity of $[Mg^{2+}\cdots CO_3^{2-}]$ ionic pairs that are trapped in the cooled $NaNO_3$ melt. The changes observed are reversible, i.e., the local environment of $NaNO_3$ was restored after a regeneration treatment to decompose $MgCO_3$ to MgO. The ex situ Na K-edge XAS experiments were complemented by ex situ magic-angle spinning ^{23}Na nuclear magnetic resonance (MAS ^{23}Na NMR), Mg K-edge XAS and X-ray powder diffraction (XRD). These additional experiments support our interpretation of the Na K-edge XAS data. Furthermore, we develop in situ Na (and Mg) K-edge XAS experiments during the carbonation of the sorbent ($NaNO_3$ is molten under the conditions of the in situ experiments). These in situ Na K-edge XANES spectra of molten $NaNO_3$ open new opportunities to investigate the atomic scale structure of CO_2 sorbents modified with Na-based molten salts by using XAS.

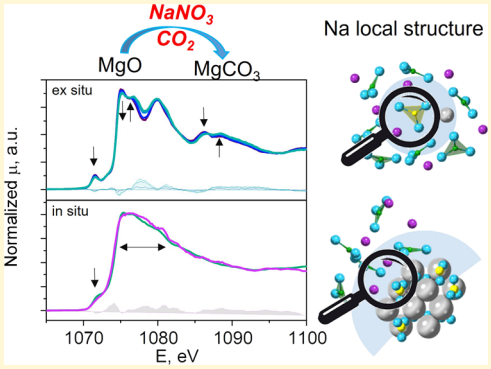

1. INTRODUCTION

The rising concentration of CO_2 in the atmosphere resulting largely from the combustion of fossil fuels is the major cause of global warming.[1,2] In this context, the development and deployment of technologies for CO_2 capture and storage (CCS) is key to limit the global temperature increase below the 2 °C target.[3,4] Yet, postcombustion and precombustion CCS techniques rely on the availability of efficient and cost-effective CO_2 sorbents.[5] The most mature CCS technology that is applied on a large scale to capture CO_2 from natural gas is amine scrubbing. However, amine scrubbing has some drawbacks, such as the production of toxic components and a large energy penalty due to the high water content in the solvent. Hence, as a more cost-effective alternative, solid CO_2 sorbents based on metal oxides have been proposed. In this context, MgO-based CO_2 sorbents (via $MgO + CO_2 \leftrightarrow MgCO_3$, $\Delta H_{300K} = -106.05$ kJ mol^{-1})[6] offer several advantages such as intermediate temperature operation (250−450 °C),[7] natural abundance,[8] environmentally benign nature,[9] and a high theoretical CO_2 capacity (1.09 g_{CO_2}/g_{MgO}).[10,11] However, due to the slow carbonation kinetics of pristine MgO, the addition of promoters such as molten alkali metal salts (AMSs, typically alkali metal nitrates) is required to ensure practically relevant CO_2 uptakes.[12−16]

There have been a series of studies that have explored the role and functioning of promoters on the CO_2 uptake of MgO-based CO_2 absorbents.[11,14−22] It has been proposed that MgO dissolves in the molten AMS promoter as $[Mg^{2+}\cdots O^{2-}]$ ionic pairs.[14−16,22] Zhang et al. hypothesized that CO_2 is adsorbed at the triple phase boundary (TPB) between solid MgO, liquid AMS, and gaseous CO_2.[16] The adsorbed CO_2 then reacts with $[Mg^{2+}\cdots O^{2-}]$ ionic pairs to form $[Mg^{2+}\cdots CO_3^{2-}]$ ionic pairs at the TPB.[16] However, Jo et al. disproved the critical role of TPBs based on a control experiment using a MgO wafer that was completely covered with $NaNO_3$ (avoiding the presence of any TPB) and that was subjected to a carbonation treatment.[22] The analysis of the treated wafer (after washing out the $NaNO_3$ coating) by Fourier-transform infrared spectroscopy (FT-IR) revealed carbonate formation despite the absence of any TPB.[22] Hence, an alternative mechanism was proposed in which gaseous CO_2 dissolves in the molten salt[23] and reacts with O^{2-}

Received: August 16, 2023
Revised: November 15, 2023
Accepted: November 15, 2023
Published: December 1, 2023

ions present in the molten salt (O^{2-} are formed either from the dissociation of the nitrate group via $NO_3^- \rightarrow NO_2^+ + O^{2-}$[14,21] or from MgO dissolution)[22] producing CO_3^{2-} ions.[24] Upon reaching supersaturation of $[Mg^{2+}\cdots CO_3^{2-}]$ ionic pairs in the melt, the precipitation of crystalline $MgCO_3$ takes place.[11] Further, it was found that $MgCO_3$ grows at the interface between MgO and $NaNO_3$ according to grazing incident diffraction and electron microscopy studies on a model MgO(100) single crystal coated with molten $NaNO_3$.[17] More recently, using density functional theory (DFT) calculations and ^{18}O labeling experiments, it was hypothesized that the carbonation mechanism of $NaNO_3$-promoted MgO involves the rapid formation of surface carbonates followed by their dissolution, yielding $[Mg^{2+}\cdots CO_3^{2-}]$ ion pairs dissolved in the AMS melt, and oxygen of NO_3^- groups do not participate in carbonation reaction.[20]

Despite the new insights gained into the mechanism of CO_2 uptake in alkali metal-promoted MgO, there is still little understanding of the local structure of the molten salt promoter under realistic carbonation conditions. This lack of knowledge is because the promoter is molten under reaction conditions, and only a few experimental techniques can probe the local structure of the molten salt under reactive conditions. Previous related studies have investigated the structure of (bare) molten alkaline nitrates via X-ray total scattering in combination with molecular dynamics simulations.[18,25,26] However, due to the presence of multiple phases in the CO_2 sorbents under reaction conditions (i.e., MgO, $MgCO_3$, and the molten nitrate), X-ray total scattering studies are not well-suited to study the local structure of molten promoters such as $NaNO_3$ under CO_2 capture conditions. In view of these challenges, element-selective techniques such as X-ray absorption spectroscopy (XAS) are highly suitable to probe the local structure around a specific element (such as Na) in multiphase systems. Yet, Na K-edge XAS studies under realistic CO_2 capture conditions face considerable experimental challenges because the X-ray absorption edge of Na is in the soft/tender X-ray region (0.2 to ∼2 keV, Na K-edge 1.08 keV). Soft/tender X-rays are poorly transmitted through matter (i.e., through air or reaction cells), hence experiments must be performed under vacuum.[27,28] Studies that apply Na K-edge XAS on CO_2 capture materials are scarce,[29,30] and experimental developments are required to exploit the full potential of this technique in the field of CO_2 sorbents.

In this work, we explore Na K-edge XAS to probe the local environment of Na in $NaNO_3$-promoted, MgO-based CO_2 sorbents. First, we investigate ex situ Na K-edge XAS data at room temperature to (indirectly) probe changes in the Na environment during CO_2 uptake conditions (i.e., during MgO carbonation). These experiments were complemented by ex situ structural characterization techniques including Mg K-edge XAS analysis, X-ray powder diffraction (XRD), and magic-angle spinning nuclear magnetic resonance (MAS ^{23}Na NMR). Next, an experimental setup that allows the collection of in situ XAS data at the Na and Mg K-edges under carbonation conditions was designed and constructed, allowing the acquisition of XAS data of $NaNO_3$-promoted MgO for the first time. Both ex situ and in situ analysis reveal changes in the local structure around Na upon carbonation. We attribute the changes observed (both in situ and ex situ) to a restructuring (both in a liquid and in a solid state) at the $NaNO_3/MgCO_3$ interfaces and possibly in the vicinity of $[Mg^{2+}\cdots CO_3^{2-}]$ ionic pairs dissolved in the $NaNO_3$.

2. EXPERIMENTAL SECTION

2.1. Materials. *2.1.1. Sorbent Synthesis.* The CO_2 sorbent MgO−10$NaNO_3$ was prepared from hydromagnesite $Mg_5(CO_3)_4(OH)_2 \cdot 4H_2O$ (Acros Organics, extra pure) and $NaNO_3$ (Sigma-Aldrich, ≥99.5%) by a wet mixing procedure described elsewhere (here the "10" in the sorbent name definition refers to the moles of Na per 100 mol of Mg in the sorbent).[11]

2.1.2. Carbonation Treatment. The preparation of carbonated samples for ex situ structural analysis (vide infra) was carried out in a TGA DSC 3+ instrument (Mettler Toledo). Here, approximately ∼100 mg of a sample was placed in a crucible and pretreated in N_2 (1 bar, 80 mL min^{-1}) for 30 min at 450 °C to yield a material that is referred to as the as-prepared sample (MgO−10$NaNO_3$_as-prep). Next, the as-prepared sample was cooled down to 315 °C and subjected to a carbonation treatment in CO_2 (1 bar, 80 mL min^{-1}) for 5, 25, and 55 min to yield samples with varying degrees of carbonation being referred to as MgO−10$NaNO_3$_carb5, MgO−10$NaNO_3$_carb25, and MgO−10$NaNO_3$_carb55, respectively. The respective regenerated material was produced by treating the MgO−10$NaNO_3$_carb55 sample for 15 min at 450 °C in N_2 (1 bar, 80 mL min^{-1}); the regenerated sample is referred to as sample MgO−10$NaNO_3$_regen (Figure S1).

2.1.3. Reference Samples. To assist the structural analysis, the following compounds were used as references: $NaNO_3$ (Sigma-Aldrich, ≥99.5%), $NaNO_2$ (Sigma-Aldrich, ≥97.0%), γ-Na_2CO_3 (Acros Organics, ≥99.5%), synthetic $Na_2Mg(CO_3)_2$, MgO, and $MgCO_3$. $Na_2Mg(CO_3)_2$ was prepared via a solid chemistry route in which hydromagnesite was thoroughly mixed with Na_2CO_3 in an agate mortar. The obtained powder was pelletized and treated at 350 °C in CO_2 for 10 h in a TGA DSC 3+ (Mettler Toledo) instrument. The treatment was repeated three times until XRD analysis showed that all of Na_2CO_3 was converted to $Na_2Mg(CO_3)_2$, with excess MgO (Section S2 of Supporting Information, Figure S2a). $MgCO_3$ was obtained from hydromagnesite via a wet chemistry route using a suspension of hydromagnesite in monoethylene glycol/water solution, which was refluxed at 150 °C in a continuous CO_2 flow (Figure S2b).[31] The MgO reference was produced by calcination of hydromagnesite at 450 °C in air for 4 h. The crystalline phase composition of all references was confirmed by XRD.

2.2. Ex Situ Structural Analysis. *2.2.1. X-ray Powder Diffraction.* The crystalline phase composition of the CO_2 sorbent was studied by XRD. The diffractometer (Panalytical Empyrean) was equipped with a Bragg−Brentano HD mirror and operated at 45 kV and 40 mA by using Cu$K\alpha_{1,2}$ radiation. Each sample was scanned in the 2θ range of 5−90°, the step size was 0.016°, and the scan time per step was 0.68 s. Rietveld refinements were performed using the FullProf software,[32] using crystal structures previously reported and available in the Inorganic Crystal Structure Database (ICSD) database (MgO 9863, $MgCO_3$ 40,117, $NaNO_3$ 15,332, and $Na_2Mg(CO_3)_2$ 100,482, more details are given in the Section S2 of Supporting Information).

2.2.2. X-ray Absorption Spectroscopy. XAS measurements at the Na and Mg K-edges were carried out at the undulator beamline PHOENIX II (X07MB) at the Swiss Light Source (SLS, PSI, Villigen, Switzerland). Ex situ data were collected using both fluorescence (1-element Si-drift diode detector SDD, Ketek, Germany) and total electron yield (TEY) signals. The powders were supported on a copper plate by using metallic indium for fixation. The current of the incident beam (I_0) was measured as the total electron yield signal using 0.5 μm thin polyester foil coated with metallic Ni (50 nm). The energy calibration was carried out using NaCl (1075.6 eV at the inflection point).[29] Both ex situ and in situ data were processed using the software Athena as part of the Demeter software package.[33]

2.2.3. X-ray Absorption Near Edge Structure Simulation. Theoretical XANES data were simulated using the finite difference method implemented in the FDMNES code.[34,35] The crystal structure of $NaNO_3$ (ICSD: 15332) with space group $R\bar{3}c$ was used. Full potential calculations were performed in either 8.5 Å (for manual O atomic position variation) or 9 Å (for machine learning (ML) type algorithm) radius around the absorbing Na atom. The structure-spectrum relationships were obtained in PyFitIt code[36] based on a data

https://doi.org/10.1021/acs.chemmater.3c02077
Chem. Mater. 2023, 35, 10060−10069

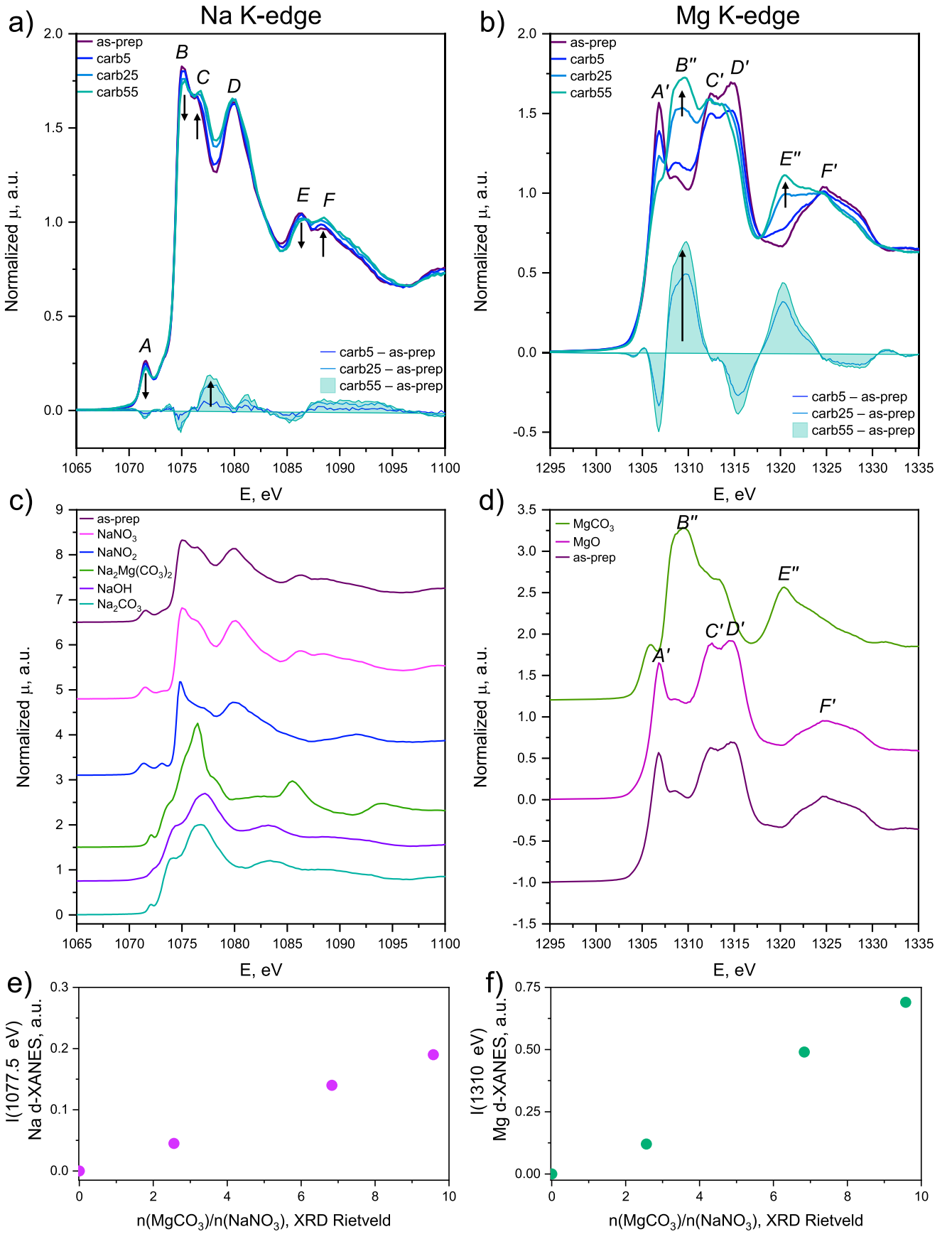

Figure 1. Ex situ XANES spectra for MgO−10$NaNO_3$_as-prep, MgO−10$NaNO_3$_carb5, MgO−10$NaNO_3$_carb25, and MgO−10$NaNO_3$_carb55 at the (a) Na K-edge and (b) Mg K-edge. XANES spectra of reference materials at the (c) Na K-edge and (d) Mg K-edge (stacked vertically for clarity).

https://doi.org/10.1021/acs.chemmater.3c02077
Chem. Mater. 2023, 35, 10060−10069

Figure 1. continued

The intensity of the feature at (e) 1077.5 eV (Na K-edge XANES) and (f) 1310 eV (Mg K-edge XANES) in the difference spectra as a function of the ratio between $MgCO_3$ and $NaNO_3$ in the material, as determined by Rietveld analysis.

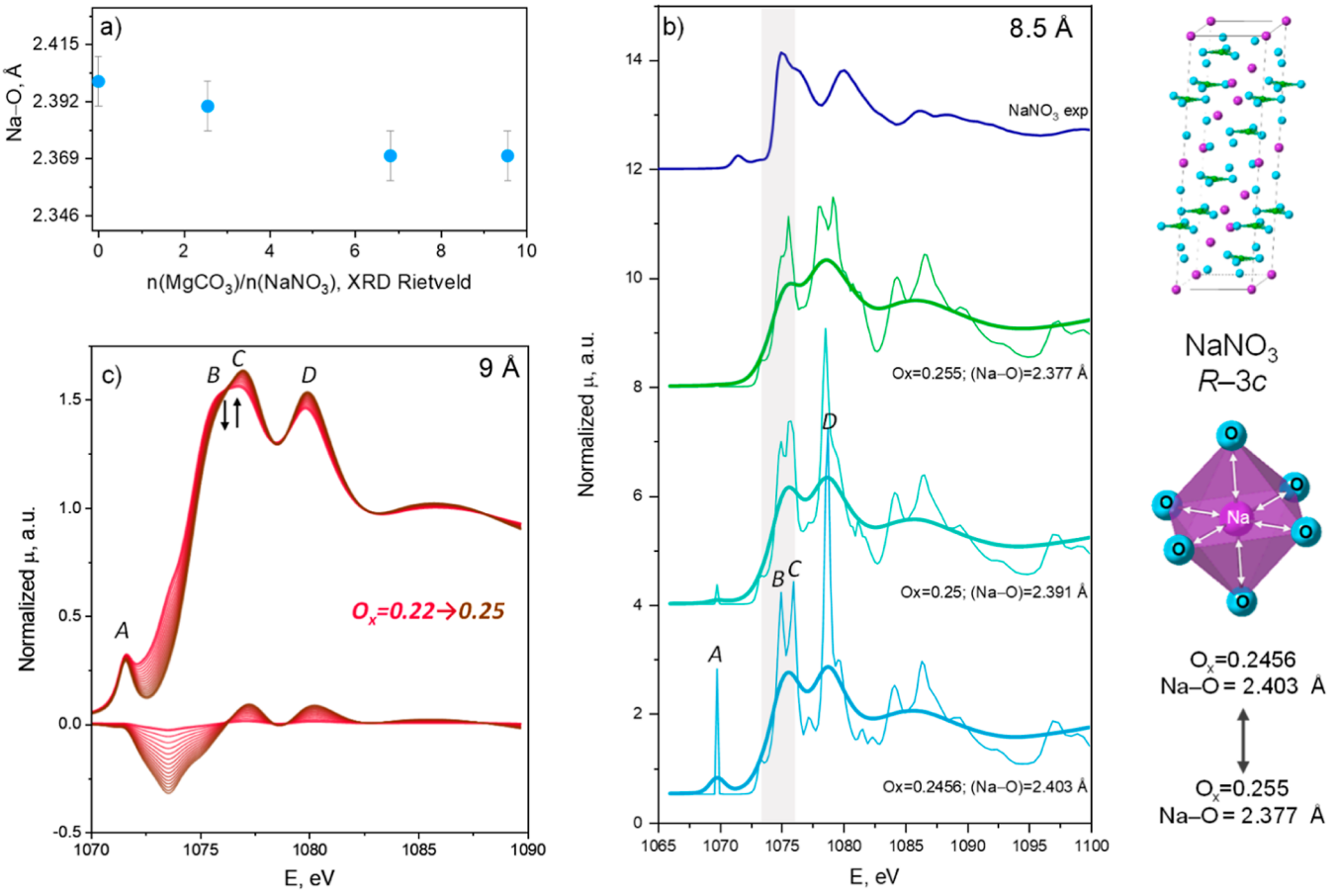

Figure 2. (a) Na−O interatomic distance obtained from EXAFS fitting vs a ratio between $MgCO_3$ and $NaNO_3$ in the samples, as determined by Rietveld refinement, (b) FDMNES simulation of the $NaNO_3$ Na K-edge XANES spectrum with varying O_x position (crystal structure based on ICSD: 15332), including the $NaNO_3$ crystal structure and the local NaO_6 octahedron, with the arrows pointing to the variation in Na−O distance upon variation of O_x position, (c) simulated Na K-edge XANES spectra of $NaNO_3$ with varying O_x (Na−O distance) using a ML type algorithm.

set of spectra for systematically varied structural parameters. More details about the simulations can be found in Supporting Information.

2.2.4. Magic-Angle Spinning Nuclear ^{23}Na Magnetic Resonance. MAS ^{23}Na NMR spectra were obtained on a Bruker Advance, 700 MHz, operating at a ^{23}Na Larmor frequency of 158.74 MHz. The measurements were performed at room temperature using a triple-resonance 3.2 mm Bruker probe, at a magic angle spinning (MAS) rate of 20 kHz, with a 2.5 μs $\pi/2$ pulse. The calibration of the chemical shift position was performed by using NaCl.

2.2.5. Scanning Transmission Electron Microscopy and Energy Dispersive X-ray. Scanning transmission electron microscopy and energy dispersive X-ray mapping were acquired using an FEI Talos F200X. The operation voltage of the instrument was set to 200 kV in STEM mode.

2.3. In Situ XANES at the Na and Mg K-Edges. To collect in situ Na and Mg XAS data during carbonation, we designed and constructed a dedicated cell (Figures 3c and S5). The cell allowed us to control the temperature (25−400 °C) and the gas flow (up to 0.4 bar of N_2 or CO_2) (Figure 3d) and was placed in a vacuum chamber at a pressure of approximately 2.5 × 10^{-4} mbar. In such experiments, the sample MgO−10$NaNO_3$ was pressed into a pellet (diameter of 9 mm and thickness of ca. 1 mm) and clamped onto a sample holder. The cell was equipped with two Si_3N_4 windows (Silson Ltd.) of 500 nm thickness: one window to allow for the transmission of the incoming beam onto the sample and the second window to allow for the collection of the fluorescence signal from the sample using a single-element Si-drift diode detector (Manufacturer Ketek, Germany). The cell contains two windows made of Si_3N_4 of 500 nm thickness mounted perpendicular to each other (further details in Figure S5). The windows were glued using a high temperature epoxy, which was applied to the window holder. One window allowed the penetration of the incoming X-ray beam into the cell and its interaction with the sample. The other window allowed the detection of X-rays in fluorescence mode (using a 1-element Si-drift diode detector). Using separate windows for the incoming and outgoing beam allows mounting the windows further away from the hot sample and hence keeping the windows at temperatures that are compatible with the epoxy resin glue. Furthermore, a flow of gaseous nitrogen was used to cool the frame, which holds the window to minimize the heating of the windows (Figure S5). The sample was pressed into a cylindrical pellet of 9 mm in diameter and about 1 mm thickness and mounted in the heated sample holder in the cell. The sample holder for the pelletized sample was placed in a 45° angle with respect to each of the two windows (Figures 3c and S5). The cell was mounted inside the vacuum chamber of the end-station of the PHOENIX II beamline.

https://doi.org/10.1021/acs.chemmater.3c02077
Chem. Mater. 2023, 35, 10060−10069

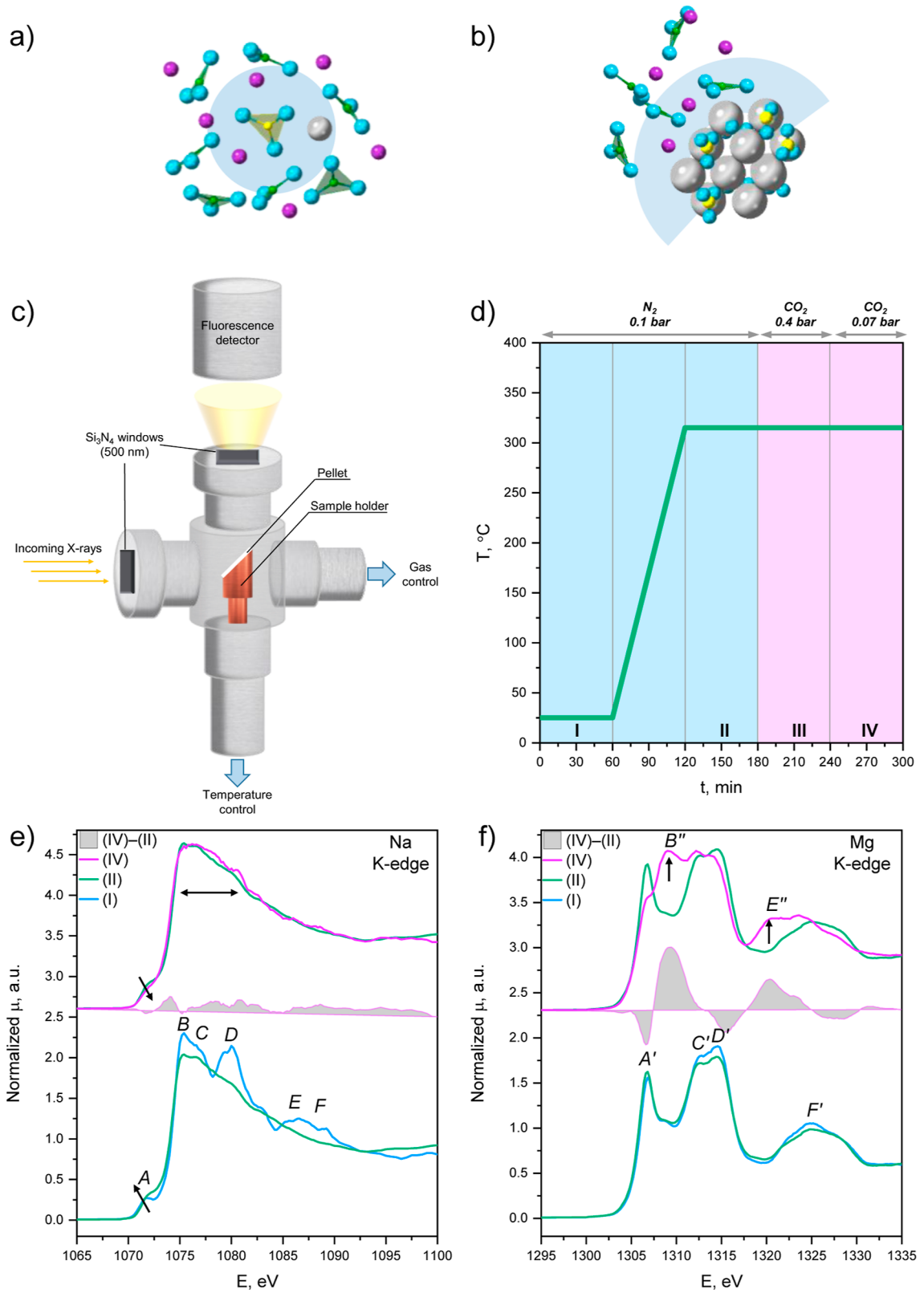

Figure 3. (a) Illustrations of the restructuring of molten $NaNO_3$ during carbonation due to (a) dissolved $[Mg^{2+}\cdots CO_3^{2-}]$ ionic pairs and the (b) $NaNO_3/MgCO_3$ interface. Color legend: blue—oxygen, purple—sodium, green—nitrogen, gray—magnesium, and yellow—carbon. (c) Schematics of the reaction cell used for collecting in situ XAS at the Na and Mg K-edges. (d) Experimental protocol for data acquisition; I—25 °C, N_2, 0.1 bar; II—315 °C, N_2, 0.1 bar; III—315 °C, CO_2, 0.4 bar; IV—315 °C, CO_2, 0.07 bar. XANES spectra at the (e) Na K-edge and (f) Mg K-edge.

https://doi.org/10.1021/acs.chemmater.3c02077
Chem. Mater. 2023, 35, 10060−10069

3. RESULTS AND DISCUSSION

3.1. Ex Situ Structural Characterization of the As-Prepared, Carbonated, and Regenerated CO_2 Sorbents.

3.1.1. Crystalline Phase Composition. At room temperature the as-prepared MgO−10$NaNO_3$_as-prep CO_2 sorbent (pretreated at 450 °C, N_2, 80 mL min^{-1} for 30 min) contained two crystalline phases: MgO ($Fm\bar{3}m$, 83 wt %) and $NaNO_3$ ($R\bar{3}c$, 17 wt %) according to Rietveld refinements of XRD data (Section S2 in Supporting Information). The carbonated samples (at 315 °C, CO_2, 80 mL min^{-1} for 5, 25, or 55 min) contained $MgCO_3$ ($R\bar{3}c$), MgO ($Fm\bar{3}m$), and $NaNO_3$ ($R\bar{3}c$) in the following concentrations [$MgCO_3$, MgO, and $NaNO_3$]: [33, 54, and 13 wt %], [61, 30, and 9 wt %], and [76, 16, and 8 wt %] in MgO−10$NaNO_3$_carb5, MgO−10$NaNO_3$_carb25, and MgO−10$NaNO_3$_carb55, respectively. After carbonation for 55 min, a regeneration step was performed (450 °C, N_2, 80 mL min^{-1} for 15 min), that restored the initial composition of the sorbent (within errors) in MgO−10$NaNO_3$_regen CO_2 sorbent: MgO (81 wt %) and $NaNO_3$ (19 wt %).

3.1.2. Local Structure. While XRD analysis provided information about the crystalline bulk average structure, the local structure of the as-prepared, carbonated, and regenerated CO_2 sorbents was characterized by ex situ XANES at the Na and Mg K-edges, which was further complemented by MAS ^{23}Na NMR. The XANES spectra at the Na and Mg K-edges for the as-prepared and the carbonated materials are presented in Figure 1a,b, respectively. All of the features, i.e., labeled as A′ (1306.9 eV), C′ (1312.5), D′ (1314.7 eV) and F′ (1324.8 eV), that were present in the acquired Mg K-edge spectrum of MgO−10$NaNO_3$_as-prep were well-described by the MgO reference (the absorption edge corresponds to the transition of the 1s electron to unoccupied states, with single and multiple photoscattering by neighboring atoms in the nearest and outermost coordination shells contributing to the features above the edge).[37,38] During carbonation the intensity of the new features B″ (1309.3 eV) and E″ (1320.4 eV) due to $MgCO_3$ grew, indicative of an increasing fraction of $MgCO_3$ with increasing carbonation time.[39,40] The emergence and growth of features B″ and E″ were also clearly observed in the difference spectra (i.e., the difference between the spectra of a MgO−10$NaNO_3$_carbX and that of the MgO−10$NaNO_3$_as-prep sorbents) and were in line with the XRD results. To confirm that the Mg K-edge spectra of the carbonated samples could be described by two phases only, i.e., MgO and $MgCO_3$, we performed a linear combination fitting (LCF) analysis of the Mg K-edge XANES spectra. The spectra of the carbonated materials were well-described by a LCF of the two references $MgCO_3$ and MgO (Figure S7) and yielded values of molar fractions [$MgCO_3$: ($MgCO_3$ + MgO)] = 0.13, 0.45, and 0.61 in MgO−10$NaNO_3$_carb5, MgO−10$NaNO_3$_carb25, and MgO−10$NaNO_3$_carb55, respectively, that were in good agreement with XRD and TGA measurements (see comparison in Figure S8). In the regenerated sorbent, MgO−10$NaNO_3$_regen, the features due to MgO were fully restored, which was in line with the complete decomposition of $MgCO_3$ into MgO after regeneration (Figure S9b).

The Na K-edge XANES spectrum of the MgO−10$NaNO_3$_as-prep sorbent, Figure 1a, showed identical features as the spectrum of the reference $NaNO_3$ (Figure 1c). The spectrum showed characteristic features of $NaNO_3$ above the edge, i.e., B (1075.3 eV), C (1076.9 eV), D (1079.8 eV), E (1086.3 eV), and F (1088.4 eV).[41] In addition, both spectra ($NaNO_3$ and MgO−10$NaNO_3$_as-prep) exhibit pre-edge feature A (1071.8 eV).

Interestingly, the Na K-edge XANES spectra of the carbonated samples differed from those of the as-prepared material. With increasing carbonation time, the intensity of the pre-edge features A, B, and E decreased, while the intensity of features C and F increased. In addition, with increasing carbonation time, features C and D became visibly broader. The described changes in the features become clearer in the difference spectra (Figure 1a). When plotting the intensity of the features C (Na K-edge at ca. 1077.5 eV) and B″ (Mg K-edge at ca. 1310 eV) in the difference spectra against the $MgCO_3$ content (determined by Rietveld refinement), we can infer that the changes observed in the Na K-edge XANES spectra upon carbonation scaled with the quantity of $MgCO_3$ formed (Figure 1e,f). The XANES spectrum of the regenerated sample revealed that the $NaNO_3$ environment of the as-prepared sample was largely restored. Notably, the intensity of feature B increased (which was slightly higher than that in the as-prepared sample), while features A, C, E, and F were largely restored to the initial positions and intensities, indicating that the changes that occurred upon carbonation were mostly reversible (Figure S9a).

One hypothesis to explain the changes observed in the Na K-edge XANES spectra upon carbonation could be the decomposition of $NaNO_3$, e.g., into $NaNO_2$ or Na_2O which would transform further under carbonation conditions (CO_2, 315 °C) to sodium-containing carbonates Na_2CO_3 and/or $Na_2Mg(CO_3)_2$, as previously observed.[42] However, according to Rekhtina et al., the decomposition of $NaNO_3$ does not take place below 450 °C. Also, Na_2CO_3 and $Na_2Mg(CO_3)_2$ could only be formed over repeated carbonation and regeneration ($T \geq 450$ °C) cycles through the partial decomposition of $NaNO_3$ and the carbonation of the decomposition products, as previously observed by Rekhtina et al.[42] Since the carbonation temperature was considerably below the decomposition temperature (315 °C), $NaNO_3$ decomposition is not expected. In addition, we compared the XANES spectra of the carbonated sorbent with the most likely $NaNO_3$ decomposition products (under ambient or CO_2 capture conditions), i.e., Na_2CO_3, $Na_2Mg(CO_3)_2$, NaOH, and $NaNO_2$ (Figure 1c). Our analysis showed that none of these potential decomposition products explain feature C (1076.9 eV) in the carbonated samples. This is illustrated in Figure S10, which demonstrates that the Na K-edge XANES spectrum of MgO−10$NaNO_3$_carb55 was not well-described by a linear combination of the potential decomposition products. Note that neither Na_2CO_3, $Na_2Mg(CO_3)_2$, nor NaOH phases were detected by XRD (nor MAS ^{23}Na NMR, vide infra). Furthermore, the decomposition of $NaNO_3$ is an irreversible process; if there was $NaNO_3$ decomposition to occur, the initial spectrum should not be recovered in the regenerated material, which is, however the case (Figure S9a). Therefore, we discarded the hypothesis that changes in the Na K-edge XANES spectra of MgO−10$NaNO_3$ upon carbonation were due to the formation of either Na_2CO_3, $Na_2Mg(CO_3)_2$, $NaNO_2$, or NaOH. Since the cell parameters of $MgCO_3$ [e.g., a = 4.6408(4) Å and c = 15.065(1) Å for MgO−10$NaNO_3$_carb55] did not show an appreciable change with respect to the cell parameters of $MgCO_3$ reference [a = 4.64261(5) Å and c = 15.0604(2) Å], we also discarded the incorporation of Na^+ in the $MgCO_3$ crystal structure (Section S2 of Supporting Information).

Instead, we hypothesize that the changes revealed by Na K-edge XANES upon carbonation were due to changes in the Na

https://doi.org/10.1021/acs.chemmater.3c02077
Chem. Mater. 2023, 35, 10060−10069

local structure in the vicinity of $MgCO_3$, i.e., at the $NaNO_3$/$MgCO_3$ interfaces and due to the dissolution of $[Mg^{2+}\cdots CO_3^{2-}]$ ion pairs in the $NaNO_3$ melt (vide infra). Even though these XANES data did not probe directly the interfaces of our materials (yielding a sum of surface, interfaces, and bulk Na sites), if a change of the Na local structure occurred at $MgCO_3$/$NaNO_3$ interfaces, we would expect that the spectral changes increase with increasing $MgCO_3/NaNO_3$ ratios as observed for our data (Figure 1b,e,f). In this context, it is worth noting that STEM−EDX mapping showed that Na ($NaNO_3$) was well distributed throughout the CO_2 sorbent (i.e., Na and Mg EDX signals overlap spatially), yet also some sub-micrometer-sized particles were observed (Figure S11).

Na K-edge XANES experiments were complemented by MAS ^{23}Na NMR (Figure S12). The MAS ^{23}Na NMR spectrum of the as-prepared sorbent showed a single peak with a chemical shift of −15.4 ppm (Figure S12a), in line with the MAS ^{23}Na NMR signature of the reference $NaNO_3$ (Figure S12c). After carbonation, a second peak developed in the MAS ^{23}Na NMR spectra, with a chemical shift located at around −11 ppm (Figure S12a). This peak could not be ascribed to the $Na_2Mg(CO_3)_2$ or Na_2CO_3 references (Figure S12c), in line with XANES and XRD analyses (vide supra). Further, MAS ^{23}Na NMR also confirmed that the spectrum of MgO−10$NaNO_3$_regen was similar to the spectrum of MgO−10$NaNO_3$_as-prep (Figure S12b), i.e., further confirming that changes in the local environment of Na were reversible and related to the presence of $MgCO_3$ in the sample. Therefore, MAS ^{23}Na NMR data provides important additional (qualitative) evidence that the local environment around Na changes upon carbonation, while regeneration restores the initial $NaNO_3$ environment, confirming the results of the XAS analysis.

Extended X-ray absorption fine structure (EXAFS) analysis at the Na K-edge provided further insight into the change in the local environment of Na after carbonation. The Fourier transformed (FT) EXAFS data (not corrected for phase shift) exhibited a peak due to the Na−O coordination that was centered at ca. 1.9 Å and peaks due to Na−N and Na−Na coordination at ca. 3.5 and 4.7 Å, respectively (Figure S13). Due to the limited k range of the data (k_{max} = 6.8 Å^{-1} limited by the Mg K-edge energy), only the first coordination shell was fitted. The results of the fitting showed a shortening of the Na−O interatomic distance with increased degree of carbonation, i.e., Na−$O_{as\text{-}prep}$ = 2.40(1) Å and Na−O_{carb55} = 2.37(1) Å (Figure 2a) and an increase back after regeneration, i.e., Na−O_{regen} = 2.39(1) Å (Table S5). Fitting of the EXAFS data also yielded higher Debye−Waller factors (σ^2) in the carbonated samples, which might indicate a higher degree of structural disorder in Na−O coordination upon carbonation. However, it should be noted that the errors in the σ^2 fitted are high.[43] Similar trends were obtained for the Na−O distances (and σ^2) when fitting in *R*-space (FT) or in *k*-space as shown in Figure 2a (i.e., using the back FT in the range between 1.2 and 2.6 Å, Figure S16) confirming the reproducibility of the fittings (Tables S5 and S6). To summarize, EXAFS analysis also indicated that the local structure around Na underwent changes upon carbonation, in line with Na K-edge XANES and MAS ^{23}Na NMR data.

Next, we turn to a theoretical analysis of the Na K-edge XANES spectra. The ab initio simulations of XANES was carried out in FDMNES code (more details are given in Section S8 of Supporting Information).[34] The nonstructural parameters of the calculation were obtained by reproducing the spectrum of $NaNO_3$ reference (Figure S19c). Next, to explain the spectral variation observed in the carbonated materials, we attempted to establish the dependency of XANES upon the Na−O distance, based on the changes obtained in the EXAFS analysis. Starting from the crystal structure of $NaNO_3$, the atomic position *x* of the oxygen atom (referred to as O_x herein for convenience, Table S7, Figures 2b and S3) was varied. An increase in O_x from 0.2456 (Na−O = 2.403 Å) to 0.25 (Na−O = 2.391 Å) (Table S8) led to clear changes in the XANES spectra, viz., an intensification of feature C and a decrease in the intensity of feature B (Figure 2b). A further increase of the O_x position to 0.255 (Na−O = 2.377 Å) resulted in further intensification of feature C and lowering of feature B. Additionally, we employed a machine learning (ML) type algorithm trained on the theoretical spectra of $NaNO_3$ with systematic variation of O_x coordinate range [0.146−0.346] and cell parameters a [4.97−5.17] and c [16.7−16.9], which allowed prediction of XANES spectra for any combination of these parameters (Figure 2c, more details in Section S8 of Supporting Information). These results also showed how the shortening of the Na−O distance resulted in spectral changes resembling the ones observed in carbonated samples (Figure 1a). The Rietveld analysis of the XRD data did not reveal a similar trend of an O_x increase in the carbonated samples (Tables S3 and S4). Since XRD analysis relies solely on coherent X-ray scattering, it does not probe changes in the local structure that are related to imperfections in the material. Thus, the combined XAS and XRD analyses support the conclusion that the observed changes in the Na environment were not due to changes in the crystal (average) structure of $NaNO_3$. Instead, these analyses indicated the occurrence of changes in the local structure of disordered regions upon carbonation (e.g., at the interfaces between $NaNO_3$ and $MgCO_3$).

To summarize, the combined analysis of Na K-edge XANES, EXAFS, MAS ^{23}Na NMR, STEM−EDX, and XRD data revealed that the local environment around Na was altered by the presence of carbonate species ($MgCO_3/[Mg^{2+}\cdots CO_3^{2-}]$ ionic pairs). Although we currently lack a detailed atomic-scale model, the correlation between the magnitude of the changes in the XANES spectra and the $NaNO_3/MgCO_3$ ratio suggests that the observed changes in the Na environment are related to the $NaNO_3/MgCO_3$ interfaces and due to the dissolution of $[Mg^{2+}\cdots CO_3^{2-}]$ ionic pairs in the molten salt.[20] This hypothesis can be rationalized in light of previous studies showing that $MgCO_3$ nucleates and grows at the buried interface between solid MgO and molten $NaNO_3$ via the dissolution of $[Mg^{2+}\cdots CO_3^{2-}]$ ion pairs in the melt $[Na\cdots NO_3^-]$. Thus, it is likely that as $MgCO_3$ crystallites form, $NaNO_3$ remains in intimate contact with $MgCO_3$ due to the formation of a $NaNO_3$ solvation shell around $MgCO_3$. We propose that such dissolution (solvation) modifies the Na local structure in the melt and such structural modifications remain when the material is cooled (as $NaNO_3$ dispersed at the $MgCO_3$ surface and/or trapped within $MgCO_3$ as inclusions), as schematized in Figure 3a,b. This interpretation is in line with recent studies that proposed that the mechanism of CO_2 uptake in $NaNO_3$-promoted MgO proceeds through the dissolution of $[Mg^{2+}\cdots CO_3^{2-}]$ ionic pairs in the $NaNO_3$ melt (these pairs precipitate upon supersaturation yielding crystalline $MgCO_3$).[20]

3.2. In Situ Na and Mg K-Edge XANES. Lastly, we probed the local structure around Na and changes thereof during carbonation in the sorbent MgO−10$NaNO_3$ under operating conditions using in situ XANES. Such XANES measurements were performed using a custom-made cell to allow the collection of soft XAS data at high temperature (maximum tested

https://doi.org/10.1021/acs.chemmater.3c02077
Chem. Mater. 2023, 35, 10060−10069

temperature of 400 °C) and under a gas flow of N_2 or CO_2. A schematic of the cell is given in Figure 3c, and its details are described in the Experimental Section.

In situ Na and Mg K-edge XANES spectra were collected within a single experiment in a consecutive fashion (Figure 3e,f). The spectra collected at room temperature (I, Figure 3e,f) agreed with the ex situ data reported in Figure 1a,b, albeit having a lower signal-to-noise ratio, confirming the well-functioning of the in situ set up. When heating to 315 °C in N_2 (II, Figure 3e,f), the Mg K-edge XANES spectrum did not undergo significant changes with respect to the spectrum acquired at room temperature. This was expected as MgO remains in its crystalline form under these conditions. The possible dissolution of $[Mg^{2+}\cdots O^{2-}]$ ionic pairs into the melt was not identified in these experiments very likely because their concentration is below the sensitivity of our measurements, which is dominated by the crystalline MgO signal. In the Na K-edge XANES spectrum of MgO−10$NaNO_3$ collected at 315 °C in N_2, the features became broader and less intense compared to the spectrum acquired at room temperature due to the increasing thermal and structural disorder attributed to the melting of $NaNO_3$. Despite the broader features, the Na K-edge XANES spectrum of the molten salt maintained some similarities to its crystalline state. Specifically, the pre-edge feature A remained present in the spectrum of the molten state, while its intensity slightly increased with respect to that of solid $NaNO_3$, possibly due to a higher degree of structural distortion around Na or a slight decrease in the average coordination number.[44−46] Furthermore, features B−D were also clearly observed in molten $NaNO_3$, yet the relative intensity of these features differed from those in crystalline $NaNO_3$ suggesting a remaining local ordering of the NO_3^- ions around Na^+ ions in molten $NaNO_3$. Features E and F disappeared, which was related to the loss of medium and long-range order around the Na^+ ion.[47] When we compared the experimental XANES spectrum of molten $NaNO_3$ with our simulations of the $NaNO_3$ spectra when varying the cluster size (Figures S19 and S21), we could estimate the size of the local ordering. The experimental spectrum of molten $NaNO_3$ showed some resemblance (based on the overall spectral shape) to the simulated Na K-edge XANES spectrum of $NaNO_3$ using CS = 4.1 Å (using a CS of 4.1 Å in the simulation includes the first and second Na−O coordination shell, the first Na−N and the first Na−Na coordination shell, Figures S19 and S21). The simulated Na K-edge spectrum of $NaNO_3$ reproduced features A-C and the low intensity feature D of the experimental spectrum. However, the experimental spectrum showed broader features due to the high degree of disorder of $NaNO_3$ in the molten state. Although our simplified analysis does not consider the dynamics of the local Na structures, these observations are qualitatively in line with previous total scattering and molecular dynamics simulations studies of molten $NaNO_3$ structures, which show that the most intense interatomic correlations of molten $NaNO_3$ are below ca. 8 Å (i.e., local ordering), while there is no medium and long-range order.[18,25,48] These studies have shown that the first Na−O distance in molten $NaNO_3$ is positioned at 2.5−2.7 Å compared with ca. 2.4 Å in crystalline $NaNO_3$,[18,25,48] and a coordination number of 5.6 was reported, compared to 6 in crystalline $NaNO_3$.[25]

Next, the sorbent was exposed to 0.4 bar of CO_2 to carbonate the sample (III in Figure 3d) for about 60 min. During XANES spectra collection, the partial pressure of CO_2 was reduced to 0.07 bar (IV), i.e., to reduce the absorption of soft X-rays due to CO_2 in the area between the sample and the windows. Importantly, the appearance of the features B″ (1309.3 eV) and E″ (1320.4 eV) in the Mg K-edge XANES spectrum (Figure 3f) confirmed the formation of $MgCO_3$, in line with ex situ measurements (vide supra). Interestingly, the in situ experiments also showed some changes, albeit being small, in the Na K-edge XANES spectrum during carbonation (Figure 3e). Specifically, the spectrum broadened with respect to the spectrum prior to carbonation, and the intensity of the pre-edge feature decreased. These changes can be visualized better in the difference spectrum highlighted in gray in Figure 3e and are qualitatively in agreement with the observed changes in the ex situ Na K-edge XANES measurements when comparing the as-prepared and carbonated samples (Figure S22). However, due to the higher degree of disorder in the molten phase, the changes were less resolved and subtler than shown by the ex situ data. Nevertheless, it is possible that the changes observed in the in situ Na K-edge XANES spectrum upon carbonation were due to changes in the local environment/structure around Na due to the presence of $[Mg^{2+}\cdots CO_3^{2-}]$ pairs dissolved in the $NaNO_3$ melt and/or due to a solvation shell around $MgCO_3$ (as shown schematically in Figure 3a,b).[49−51] More experiments and modeling studies are required to further test this hypothesis. However, we believe that the present study provides an innovative experimental approach and important data pointing toward the validity of the CO_2 uptake mechanism in $NaNO_3$-promoted MgO as proposed by Landuyt et al.[20]

4. CONCLUSIONS

Ex situ analysis of XAS at the Na K-edge and MAS ^{23}Na NMR data of a $NaNO_3$-promoted MgO-based sorbent showed that the local structure around Na changed upon CO_2 capture, i.e., upon formation of $MgCO_3$. Quantitative EXAFS analysis revealed that the average Na−O distance decreased with increasing $MgCO_3$ content, i.e., increasing amount of CO_2 captured. Furthermore, the observed changes in the Na K-edge XANES spectra during carbonation scaled with the amount of $MgCO_3$ formed, in line with the MAS ^{23}Na NMR results. We rationalize our experimental observation of a change in the local structure of Na during carbonation as being due to the formation of $NaNO_3/MgCO_3$ interfaces and/or of the trapping of $[Mg^{2+}\cdots CO_3^{2-}]$ ionic pairs in the $NaNO_3$ melt after cooling. Such local structures differ from the local structure of Na in bulk $NaNO_3$. Moreover, the Na local structure of $NaNO_3$ was restored in the regenerated material (i.e., after $MgCO_3$ decomposed to MgO), further confirming that the observed changes were reversible and related to the presence of $MgCO_3$. Furthermore, using a customized reaction cell, we carried out in situ XAS measurements at the Na and Mg K-edges under operating conditions (i.e., during carbonation). Na K-edge XANES spectra of $NaNO_3$-promoted MgO-based sorbents whereby $NaNO_3$ was molten under in situ conditions are reported here for the first time. These in situ experiments also suggested changes in the Na K-edge XANES spectra, albeit the changes being smaller than the changes observed in the ex situ data when the sorbent was exposed to CO_2. The in situ formation of $MgCO_3$ was confirmed by Mg K-edge XANES data collected sequentially with the Na XANES data.

■ ASSOCIATED CONTENT

Supporting Information

The Supporting Information is available free of charge at https://pubs.acs.org/doi/10.1021/acs.chemmater.3c02077.

https://doi.org/10.1021/acs.chemmater.3c02077
Chem. Mater. 2023, 35, 10060−10069

Thermogravimetric analysis (TGA), X-ray powder diffraction (XRD) data, Rietveld refinements, experimental set up to acquire in situ X-ray absorption spectroscopy (XAS) data at the Na and Mg K-edges, scanning transmission electron microscopy and energy dispersive X-ray (STEM−EDX), ab initio simulations of XANES spectra, fitting of the extended X-ray absorption fine structure (EXAFS), and magic-angle spinning ^{23}Na nuclear magnetic resonance (MAS ^{23}Na NMR) (PDF)

AUTHOR INFORMATION

Corresponding Authors

Thomas Huthwelker − *Paul Scherrer Institute, 5232 Villigen PSI, Switzerland*; Email: thomas.huthwelker@psi.ch

Paula M. Abdala − *Laboratory of Energy Science and Engineering, Department of Mechanical and Process Engineering, ETH Zürich, 8092 Zürich, Switzerland*; orcid.org/0000-0002-2011-1707; Email: abdalap@ethz.ch

Christoph R. Müller − *Laboratory of Energy Science and Engineering, Department of Mechanical and Process Engineering, ETH Zürich, 8092 Zürich, Switzerland*; orcid.org/0000-0003-2234-6902; Email: muelchri@ethz.ch

Authors

Margarita Rekhtina − *Laboratory of Energy Science and Engineering, Department of Mechanical and Process Engineering, ETH Zürich, 8092 Zürich, Switzerland*

Aram Bugaev − *Paul Scherrer Institute, 5232 Villigen PSI, Switzerland*

Matthew T. Dunstan − *Department of Chemistry, University of Cambridge, Cambridge CB2 1EW, U.K.*

Alessandro Dal Pozzo − *Laboratory of Energy Science and Engineering, Department of Mechanical and Process Engineering, ETH Zürich, 8092 Zürich, Switzerland; Laboratory of Industrial Safety and Environmental Sustainability, Department of Civil, Chemical, Environmental and Materials Engineering, Alma Mater, Studiorum—Università di Bologna, 40131 Bologna, Italy*; orcid.org/0000-0003-4890-4407

Manouchehr Nadjafi − *Laboratory of Energy Science and Engineering, Department of Mechanical and Process Engineering, ETH Zürich, 8092 Zürich, Switzerland*; orcid.org/0000-0001-6652-6484

Camelia Borca − *Paul Scherrer Institute, 5232 Villigen PSI, Switzerland*

Complete contact information is available at: https://pubs.acs.org/10.1021/acs.chemmater.3c02077

Notes

The authors declare no competing financial interest.

ACKNOWLEDGMENTS

We would like to thank the Swiss National Science Foundation (SNSF) for funding under Grant 200020_156015. This project has also received funding from the European Research Council under the European Union's Horizon 2020 research and innovation program Grant Agreement 819573 and the Fondation Claude et Giuliana. The Light Source at Paul Scherrer Institut, Villigen PSI, Switzerland is acknowledged for providing access to beam time to the PHOENIX beamline through Proposal 20180697. We thank Reto Wetter for the assistance in construction and testing of the in situ XAS cell. We thank Dr. Agnieszka Kierzkowska for collecting TEM data and Dr. Alexander Yakimov for insightful discussions on NMR data.

REFERENCES

(1) Barnola, J.-M.; Raynaud, D.; Korotkevich, Y. S.; Lorius, C. Vostok ice core provides 160,000-year record of atmospheric CO_2. *Nature* **1987**, *329* (6138), 408−414.

(2) Trends in Atmospheric Carbon Dioxide. https://gml.noaa.gov/ccgg/trends/ (accessed 2023-10−08), NOAA/ESRL.

(3) International Energy Agency. *CO_2 Emissions from Fuel Combustion—Highlights*; IEA Publications: Paris, 2017.

(4) *IPCC, 2021: Climate Change 2021: The Physical Science Basis. Contribution of Working Group I to the Sixth Assessment Report of the Intergovernmental Panel on Climate Change*; Masson-Delmotte, V.; Zhai, P.; Pirani, A.; Connors, S. L.; Péan, C.; Berger, S.; Caud, N.; Chen, Y.; Goldfarb, L.; Gomis, M. I.; Huang, M.; Leitzell, K.; Lonnoy, E.; Matthews, J. B. R.; Maycock, T. K.; Waterfield, T.; Yelekçi, O.; Yu, R.; Zhou, B., Ed.; Cambridge University Press, 2021.

(5) Asia-Pacific Economic Cooperation. *Building Capacity for CO_2 Capture and Storage in the APEC Region*; Asia-Pacific Economic Cooperation, 2012.

(6) Duan, Y.; Zhang, K.; Li, X. S.; King, D. L.; Li, B.; Zhao, L.; Xiao, Y. J. Ab initio thermodynamic study of the CO_2 capture properties of M_2CO_3 (M= Na, K)-and $CaCO_3$-promoted MgO sorbents towards forming double salts. *Aerosol Air Qual. Res.* **2014**, *14* (2), 470−479.

(7) Hassanzadeh, A.; Abbasian, J. Regenerable MgO-based sorbents for high-temperature CO_2 removal from syngas: 1. Sorbent development, evaluation, and reaction modeling. *Fuel* **2010**, *89* (6), 1287−1297.

(8) Goff, F.; Lackner, K. Carbon dioxide sequestering using ultramafic rocks. *Environ. Geosci.* **1998**, *5* (3), 89−102.

(9) Pilarska, A. A.; Klapiszewski, Ł.; Jesionowski, T. Recent development in the synthesis, modification and application of $Mg(OH)_2$ and MgO: A review. *Powder Technol.* **2017**, *319*, 373−407.

(10) Zhao, X.; Ji, G. Z.; Liu, W.; He, X.; Anthony, E. J.; Zhao, M. Mesoporous MgO promoted with $NaNO_3$/$NaNO_2$ for rapid and high-capacity CO_2 capture at moderate temperatures. *Chem. Eng. J.* **2018**, *332*, 216−226.

(11) Dal Pozzo, A.; Armutlulu, A.; Rekhtina, M.; Abdala, P. M.; Müller, C. R. CO_2 Uptake and Cyclic Stability of MgO-Based CO_2 Sorbents Promoted with Alkali Metal Nitrates and Their Eutectic Mixtures. *ACS Appl. Energy Mater.* **2019**, *2* (2), 1295−1307.

(12) Hu, Y. C.; Guo, Y. F.; Sun, J.; Li, H. L.; Liu, W. Q. Progress in MgO sorbents for cyclic CO_2 capture: a comprehensive review. *J. Mater. Chem. A* **2019**, *7* (35), 20103−20120.

(13) Vu, A. T.; Park, Y.; Jeon, P. R.; Lee, C. H. Mesoporous MgO sorbent promoted with KNO_3 for CO_2 capture at intermediate temperatures. *Chem. Eng. J.* **2014**, *258*, 254−264.

(14) Harada, T.; Simeon, F.; Hamad, E. Z.; Hatton, T. A. Alkali Metal Nitrate-Promoted High-Capacity MgO Adsorbents for Regenerable CO_2 Capture at Moderate Temperatures. *Chem. Mater.* **2015**, *27* (6), 1943−1949.

(15) Harada, T.; Hatton, T. A. Colloidal Nanoclusters of MgO Coated with Alkali Metal Nitrates/Nitrites for Rapid, High Capacity CO_2 Capture at Moderate Temperature. *Chem. Mater.* **2015**, *27* (23), 8153−8161.

(16) Zhang, K.; Li, X. S.; Li, W.-Z.; Rohatgi, A.; Duan, Y.; Singh, P.; Li, L.; King, D. L. Phase Transfer-Catalyzed Fast CO_2 Absorption by MgO-Based Absorbents with High Cycling Capacity. *Adv. Mater. Interfaces* **2014**, *1* (3), 1400030.

(17) Bork, A. H.; Rekhtina, M.; Willinger, E.; Castro-Fernandez, P.; Drnec, J.; Abdala, P. M.; Muller, C. R. Peering into buried interfaces with X-rays and electrons to unveil $MgCO_3$ formation during CO_2 capture in molten salt-promoted MgO. *Proc. Natl. Acad. Sci. U.S.A.* **2021**, *118* (26), No. e2103971118.

(18) Rekhtina, M.; Dal Pozzo, A.; Stoian, D.; Armutlulu, A.; Donat, F.; Blanco, M. V.; Wang, Z. J.; Willinger, M. G.; Fedorov, A.; Abdala, P. M.; Muller, C. R. Effect of molten sodium nitrate on the decomposition pathways of hydrated magnesium hydroxycarbonate to magnesium oxide probed by in situ total scattering. *Nanoscale* **2020**, *12* (31), 16462−16473.
(19) Bork, A. H.; Ackerl, N.; Reuteler, J.; Jog, S.; Gut, D.; Zboray, R.; Müller, C. R. Model structures of molten salt-promoted MgO to probe the mechanism of $MgCO_3$ formation during CO_2 capture at a solid-liquid interface. *J. Mater. Chem. A* **2022**, *10*, 16803−16812.
(20) Landuyt, A.; Kumar, P. V.; Yuwono, J. A.; Bork, A. H.; Donat, F.; Abdala, P. M.; Müller, C. R. Uncovering the CO_2 Capture Mechanism of $NaNO_3$-Promoted MgO by ^{18}O Isotope Labeling. *JACS Au* **2022**, *2*, 2731−2741.
(21) Gao, W.; Xiao, J.; Wang, Q.; Li, S.; Vasiliades, M. A.; Huang, L.; Gao, Y.; Jiang, Q.; Niu, Y.; Zhang, B.; et al. Unravelling the Mechanism of Intermediate-Temperature CO_2 Interaction with Molten $NaNO_3$ Salt Promoted MgO. *Adv. Mater.* **2021**, *34*, 2106677.
(22) Jo, S. I.; An, Y. I.; Kim, K. Y.; Choi, S. Y.; Kwak, J. S.; Oh, K. R.; Kwon, Y. U. Mechanisms of absorption and desorption of CO_2 by molten $NaNO_3$-promoted MgO. *Phys. Chem. Chem. Phys.* **2017**, *19* (8), 6224−6232.
(23) Sada, E.; Katoh, S.; Beniko, H.; Yoshii, H.; Kayano, M. Solubility of carbon dioxide in molten salts. *J. Chem. Eng. Data* **1980**, *25* (1), 45−47.
(24) Kust, R. Carbonate Ion Dissociation in Fused Alkali Nitrates. *Inorg. Chem.* **1964**, *3* (7), 1035−1036.
(25) Tahara, S.; Toyama, H.; Shimakura, H.; Fukami, T. Structural Analysis of Molten $NaNO_3$ by Molecular Dynamics Simulation. *EPJ Web Conf.* **2017**, *151*, 01004.
(26) Wilding, M. C.; Wilson, M.; Ribeiro, M. C.; Benmore, C. J.; Weber, J.; Alderman, O.; Tamalonis, A.; Parise, J. The structure of liquid alkali nitrates and nitrites. *Phys. Chem. Chem. Phys.* **2017**, *19* (32), 21625−21638.
(27) Xto, J.; Wetter, R.; Borca, C. N.; Frieh, C.; van Bokhoven, J. A.; Huthwelker, T. Droplet-based in situ X-ray absorption spectroscopy cell for studying crystallization processes at the tender X-ray energy range. *RSC Adv.* **2019**, *9* (58), 34004−34010.
(28) Van der Eerden, A.; van Bokhoven, J. A.; Smith, A.; Koningsberger, D. Apparatus for in situ X-ray absorption fine structure studies on catalytic systems in the energy range 1000 eV< E< 3500 eV. *Rev. Sci. Instrum.* **2000**, *71* (9), 3260−3266.
(29) Kurlov, A.; Kierzkowska, A. M.; Huthwelker, T.; Abdala, P. M.; Müller, C. R. Na_2CO_3-modified CaO-based CO_2 sorbents: the effects of structure and morphology on CO_2 uptake. *Phys. Chem. Chem. Phys.* **2020**, *22* (42), 24697−24703.
(30) Yüzbasi, N. S.; Armutlulu, A.; Huthwelker, T.; Abdala, P. M.; Müller, C. R. Na-β-Al_2O_3 stabilized Fe_2O_3 oxygen carriers for chemical looping water splitting: correlating structure with redox stability. *J. Mater. Chem. A* **2022**, *10* (19), 10692−10700.
(31) Sandengen, K.; Jøsang, L. O.; Kaasa, B. Simple method for synthesis of magnesite ($MgCO_3$). *Ind. Eng. Chem. Res.* **2008**, *47* (4), 1002−1004.
(32) Rodríguez-Carvajal, J. Recent advances in magnetic structure determination by neutron powder diffraction. *Physica B: Condensed Matter* **1993**, *192*, 55−69.
(33) Ravel, B.; Newville, M. ATHENA, ARTEMIS, HEPHAESTUS: data analysis for X-ray absorption spectroscopy using IFEFFIT. *J. Synchrotron Radiat.* **2005**, *12* (4), 537−541.
(34) Bunău, O.; Joly, Y. Self-consistent aspects of x-ray absorption calculations. *J. Condens. Matter Phys.* **2009**, *21* (34), 345501.
(35) Guda, S. A.; Guda, A. A.; Soldatov, M. A.; Lomachenko, K. A.; Bugaev, A. L.; Lamberti, C.; Gawelda, W.; Bressler, C.; Smolentsev, G.; Soldatov, A. V.; Joly, Y. Optimized Finite Difference Method for the Full-Potential XANES Simulations: Application to Molecular Adsorption Geometries in MOFs and Metal-Ligand Intersystem Crossing Transients. *J. Chem. Theory Comput.* **2015**, *11* (9), 4512−4521.
(36) Martini, A.; Guda, S. A.; Guda, A. A.; Smolentsev, G.; Algasov, A.; Usoltsev, O.; Soldatov, M. A.; Bugaev, A.; Rusalev, Y.; Lamberti, C.; Soldatov, A. V. PyFitit: The software for quantitative analysis of XANES spectra using machine-learning algorithms. *Comput. Phys. Commun.* **2020**, *250*, 107064.
(37) Yoshida, T.; Tanaka, T.; Yoshida, H.; Funabiki, T.; Yoshida, S.; Murata, T. Study of Dehydration of Magnesium Hydroxide. *J. Phys. Chem.* **1995**, *99* (27), 10890−10896.
(38) Yoshimura, T.; Tamenori, Y.; Iwasaki, N.; Hasegawa, H.; Suzuki, A.; Kawahata, H. Magnesium K-edge XANES spectroscopy of geological standards. *J. Synchrotron Radiat.* **2013**, *20* (5), 734−740.
(39) Cusack, M.; Pérez-Huerta, A.; Janousch, M.; Finch, A. A. Magnesium in the lattice of calcite-shelled brachiopods. *Chem. Geol.* **2008**, *257* (1−2), 59−64.
(40) Xto, J. M.; Du, H.; Borca, C. N.; Amstad, E.; van Bokhoven, J. A.; Huthwelker, T. J. C. G. Tuning the Incorporation of Magnesium into Calcite during Its Crystallization from Additive-Free Aqueous Solution. *Cryst. Growth Des.* **2019**, *19* (8), 4385−4394.
(41) Yoshimura, T.; Tamenori, Y.; Suzuki, A.; Kawahata, H.; Iwasaki, N.; Hasegawa, H.; Nguyen, L. T.; Kuroyanagi, A.; Yamazaki, T.; Kuroda, J.; Ohkouchi, N. Altervalent substitution of sodium for calcium in biogenic calcite and aragonite. *Geochim. Cosmochim. Acta* **2017**, *202*, 21−38.
(42) Rekhtina, M.; Krödel, M.; Wu, Y.-H.; Kierzkowska, A.; Donat, F.; Abdala, P. M.; Müller, C. R. Deciphering the structural dynamics in molten salt-promoted MgO-based CO_2 sorbents and their role in the CO_2 uptake. *Sci. Adv.* **2023**, *9* (26), No. eadg5690.
(43) Galib, M.; Baer, M.; Skinner, L.; Mundy, C.; Huthwelker, T.; Schenter, G.; Benmore, C.; Govind, N.; Fulton, J. L. Revisiting the hydration structure of aqueous Na^+. *J. Chem. Phys.* **2017**, *146* (8), 084504.
(44) Neuville, D. R.; Cormier, L.; Flank, A.-M.; Prado, R. J.; Lagarde, P. Na K-edge XANES spectra of minerals and glasses. *EJM* **2004**, *16* (5), 809−816.
(45) McIntosh, G. J.; Chan, A. Probing hydrogen bonding interactions and impurity intercalation in gibbsite using experimental and theoretical XANES spectroscopy. *Phys. Chem. Chem. Phys.* **2018**, *20* (37), 24033−24044.
(46) Kulka, A.; Marino, C.; Walczak, K.; Borca, C.; Bolli, C.; Novák, P.; Villevieille, C. Influence of Na/Mn arrangements and P2/P′2 phase ratio on the electrochemical performance of Na_xMnO_2 cathodes for sodium-ion batteries. *J. Mater. Chem. A* **2020**, *8* (12), 6022−6033.
(47) Neuville, D. R.; Ligny, D. d.; Cormier, L.; Henderson, G. S.; Roux, J.; Flank, A.-M.; Lagarde, P. The crystal and melt structure of spinel and alumina at high temperature: An in-situ XANES study at the Al and Mg K-edge. *Geochim. Cosmochim. Acta* **2009**, *73* (11), 3410−3422.
(48) Ohno, H.; Furukawa, K. Structural analysis of some molten materials by X-ray diffraction. Part 4. Alkali nitrates RNO_3 (R = Li, Na, K, Rb, Cs and Ag). *J. Chem. Soc., Faraday Trans. 1* **1978**, *74*, 297.
(49) Zobel, M.; Neder, R. B.; Kimber, S. A. Universal solvent restructuring induced by colloidal nanoparticles. *Science* **2015**, *347* (6219), 292−294.
(50) Zobel, M. Observing structural reorientations at solvent-nanoparticle interfaces by X-ray diffraction-putting water in the spotlight. *Acta Crystallogr., Sect. A: Found. Adv.* **2016**, *72* (6), 621−631.
(51) Zhang, H.; Dasbiswas, K.; Ludwig, N. B.; Han, G.; Lee, B.; Vaikuntanathan, S.; Talapin, D. V. Stable colloids in molten inorganic salts. *Nature* **2017**, *542*, 328−331.

https://doi.org/10.1021/acs.chemmater.3c02077
Chem. Mater. 2023, 35, 10060−10069